The Eruptive Flare of 15 November 1991: Preflare Phenomena

Richard C. Canfield
Physics Department, Montana State University
Bozeman, MT 59717-3840, U.S.A.

Kevin P. Reardon
Osservatorio Astronomico di Capodimonte
via Moiariello 16 Napoli, Italy 80131

Abstract.
We present and interpret observations of the preflare phase of the eruptive flare of 15 November, 1991 in NOAA AR 6919. New flux emerged in this region, indicated by arch filaments in Hα and increasing vertical flux in vector magnetograms. With increasing frequency before the eruption, transient dark Hα fibrils were observed that crossed Hα bright plage and the magnetic inversion line to extend from the region of flux emergence to the filament, whose eruption was associated with the flare. These *crossing fibrils* were dynamic, and were often associated with sites of propagating torsional motion. These sites propagated from the region of flux emergence into the filament flux system. We interpret these morphological and dynamic features in terms of relaxation after magnetic reconnection episodes which create longer field lines within the filament flux system, as envisioned in the *tether cutting* model, and transfer twist to it, as well.

Key words: Magnetic Fields, Flares, Eruptions

1. Introduction

The major solar flare of 15 November, 1991 was well observed by both Yohkoh (Ogawara *et al.*, 1991) and Mees Solar Observatory (MSO). According to Solar Geophysical Data (1991), the Hα event began at $\sim$ 22:34 UT, peaked (importance 3B) at $\sim$ 22:39 UT, and ended at $\sim$ 22:54 UT. It was classified X1.5 in X-rays, and occurred in NOAA active region 6919, at heliographic latitude S13 and longitude W19. Observations of this famous flare have been published by Sakao *et al.* (1992), Hudson *et al.* (1992), Canfield *et al.* (1992), Sakao (1994), Wuelser *et al.* (1994), and Takakura *et al.* (1995).

The Yohkoh observations used in this paper were made with the Soft X-ray Telescope (SXT) and its aspect sensor (Tsuneta *et al.*, 1991). The MSO observations consist of vector magnetograms from the Haleakala Stokes Polarimeter (HSP: Mickey, 1985) and digital Hα spectra and images from the Mees CCD Imaging Spectrograph (MCCD: Penn *et al.*, 1991). Vector magnetogram observations and reduction procedures are described in detail by Canfield *et al.* 1993.

This flare was preceded by a spectacular filament eruption. The filament showed prominent torsional motions before and during the eruption. Such motions are not unusual in active filaments (*e.g.*, Schmieder *et al.*, 1985) and filament eruptions (*e.g.*, Kurokawa *et al.*, 1987). The idea that the twist of filament magnetic fields is a factor in their eruption has long been suggested by observers (*e.g.*, Vrsnak *et al.*, 1991; Moore and Roumeliotis, 1992; Pevtsov, Canfield, and Zirin, 1996), though there is controversy among theorists and modelers (*e.g.*, Priest, 1984; van Ballegooijen and Martens, 1989; Dahlburg, Antiochos, and Zang, 1991) on whether the three-dimensional mhd kink instability is a plausible explanation.

Moore and Roumeliotis (1992), following a suggestion by Sturrock, postulated a sequence of pre-eruption events they called "tether cutting", in which magnetic buoyancy, tension, and reconnection all play a role. They drew the analogy that a filament is buoyant, and acts like a balloon. It is line-tied to the photosphere by the tension of magnetic field lines, which act like the tethers that hold a hot-air balloon to the ground before launch. When field lines that thread through a filament reconnect with those in a contiguous emerging flux system, they become longer. The longer field lines are less strongly line-tied to the photosphere. After the occurrence of enough such tether-cutting events, the filament flux system becomes globally unstable and erupts, due to the global loss of equilibrium between magnetic pressure and magnetic tension.

Another interesting idea in the literature that is noteworthy in comparison to this event is the concept, in the work of Martens and collaborators (*e.g.*, Martens and Kuin, 1989), that there is no unique trigger for filament and flare eruptions, but rather that the filament flux system is in a metastable state prior to the global loss of equilibrium that corresponds to the eruption. In this state any disturbance that is strong enough to move a filament away from its equilibrium state can trigger an eruption.

To our knowledge, a novel aspect of the flare discussed in this paper is our observation of what appears to be the propagation of twist packets into the filament flux system from adjacent emerging flux following reconnection episodes. There is ample reason to believe that magnetic flux can emerge in a twisted state (see Leka, 1996 and references therein). When such twisted emerging flux reconnects with filament flux, one must expect that their coronal twist will add algebraically, since the reconnection timescale for two thin flux tubes is much less than the Alfvén timescale for either one. In the case for which both the filament and emerging flux systems have the same handedness, the longer filement field lines created by reconnection have more twist above their

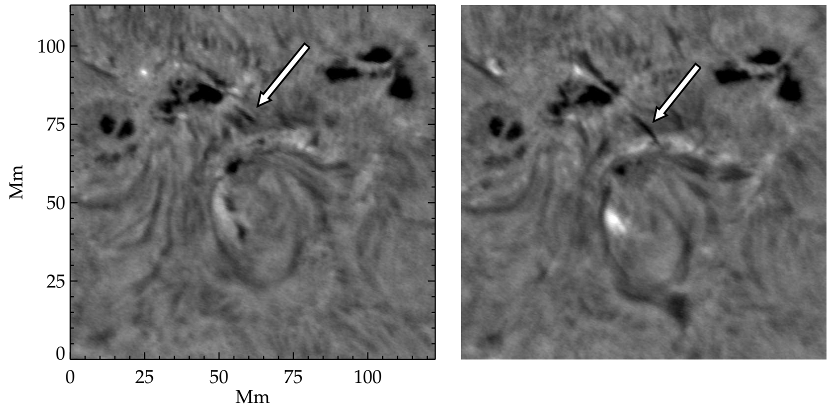

Figure 1. Selected broad-band Hα images from the MCCD monitor camera. Features indicated by arrows: Left panel – Hα arch filaments in the weak-field corridor between the filament and the positive polarity spots to the north of the filament (18:38:28 UT); Right panel – a crossing fibril, *i.e.*, a dark fibril which crosses over the bright Hα plage immediately north of the filament (19:07:41 UT). Solar north is up.

photospheric footpoints than they did prior to reconnection. An example of an event in which such a sequence of events appears to explain the subsequent eruption is the 1992 May 8 eruptive flare studied by Pevtsov, Canfield, and Zirin (1996).

2. Magnetic Flux Emergence

Two independent observations, the observation of arch filaments in Hα monitor images, on the one hand, and the observation of increasing flux in photospheric magnetograms, on the other, imply that magnetic flux emerged in the region north of the filament for at least several hours before the filament erupted. Additionally, the substantial growth of the filament early in the observing period of November 15th at MSO, relative to its size on the previous day, suggests that flux emergence was taking place overnight, as well.

One indication of flux emergence near the active-region filament is the appearance of transient dark Hα fibrils, examples of which are shown by the arrow in the left panel of Figure 1. These images are Hα filtergrams made with the MCCD monitor camera through an interference filter centered on the Hα line. Because the bandwidth of the interference is wider than the width of the Hα line, these images show both typical narrow-band Hα features (*e.g.*, chromospheric fibrils and filaments) and broad-band features (*e.g.*, sunspot umbrae and penum-

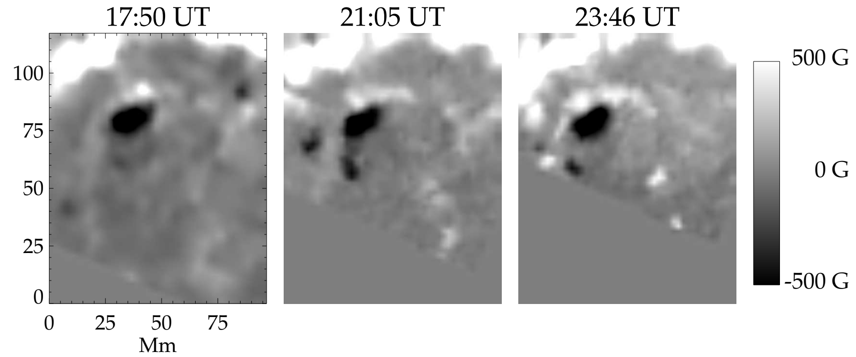

Figure 2. Vertical-field magnetograms derived from three HSP scans on the day of the flare, made using a 6″aperture: 17:50 - 18:55 UT, 200″x 170″, 5.″6 steps; 21:06 - 22:45 UT, 165″x 125″, 2.″8 steps; 23:47 - 01:26 UT, 165″x 125″, 2.″8 steps; The original data have been rotated to show solar North up.

brae). A useful feature of these and subsequent images, for orientation purposes, is the prominent row of sunspots running across the upper half of the figure. The feature of greatest interest, however, is the oval active-region filament south of them, prominent in the figure, which erupted prior to the impulsive phase of the flare. The magnetic field of the reference row of spots in the upper part of the figure is positive, whereas the spots inside the active-region filament are negative. The northwest part of the filament consists of several fingers that run out into the weak-field region west of the filament. Contiguous with the northern edge of the filament is moderately bright Hα plage. A vector magnetogram, showing that the polarity inversion line runs just north of the negative spot that is evident just inside the upper part of the oval, appears in an earlier paper (Canfield *et al.*, 1992). The arrow in the left panel of Figure 1 of the present paper indicates one of many transient dark Hα fibrils which appeared in a weak-field corridor (Klimchuk, 1987) – an area of weak field crossed by dark Hα fibrils that seem to connect opposite polarity strong fields to either side. These fibrils lie north of the oval filament and south of the row of positive spots, and appear frequently over the period of several hours before the filament eruption and flare. Such transient dark Hα fibrils, known as arch filaments, are a well-known signature of flux emergence (Zirin, 1988).

An independent indication of flux emergence is the observation of steadily increasing vertical magnetic flux in the weak-field corridor, just north of the positive spot where the flare occurred, in three successive vector magnetograms made with the HSP before, during, and after the eruption. Three vertical-field magnetograms derived from these scans are shown in Figure 2. In the upper left-hand corner of each of the three magnetograms is the positive-polarity (white) sunspot, which can be seen closest to the filament in Figure 1, east of the arrow. Closer to the center of the panels in Figure 2, in the upper-left quadrant, is a large negative-polarity (black) sunspot. This spot can be seen immediately inside the northeastern edge of the filament oval seen in Figure 1, at the 11-o'clock position of the filament imagined as a clock face. The spot is more prominent in the magnetograms than in the Hα images, in which obscuration of the photosphere by the chromosphere plays some role. In any case, the most important feature to note in Figure 2 is the increase of strong positive-polarity (white) flux as the day progresses.

Although vector magnetograms made with the HSP lack the spatial or temporal resolution required to show a one-to-one relationship between areas of increased magnetic flux and the footpoints of individual dark Hα fibrils, the spectrally well-resolved nature of the data eliminates the need for secondary calibration. We believe that the flux increase in the magnetograms shown in Figure 2 is associated with the flux emergence evidenced by the dark Hα fibrils illustrated in Figure 1, and is not an instrumental artifact.

3. Morphology and Dynamics

The impulsive phase of the 15 November flare started about 22:37 UT (Sakao *et al.*, 1992). AR 6919 was observed from 17:36 UT with the MCCD monitor and spectrograph cameras, i.e. about five hours prior to the impulsive phase, and the first vector magnetogram was started at 17:50 UT. We thus have an unusually complete record of preflare observations: from the MCCD – chromospheric and photospheric morphology (from the monitor camera) and dynamics (from the spectrograph camera); from the HSP – the photospheric magnetic field evolution. Complementing these ground-based observations are four orbits of preflare Yohkoh SXT data, the first of which started at about 16:56 UT.

3.1. Hα Imaging Spectrograph Observations: A Movie

Critical observations for this paper are those from the Mees CCD imaging spectrograph (Penn *et al.*, 1991). The MCCD scans were made with its standard Hα flare setup: spectrograph camera spatial field of view $\sim 3' \times 4'$, $2.''4$ pixels, 18.7 Å spectral range, 113 mÅ pixels, completing one scan and one broad-band Hα monitor image each 15 s. Though the spatial resolution of MCCD spectroheliograms is low relative to the broad-band Hα filtergrams at times of good seeing, the Hα profiles bring important diagnostic advantages. The most important observed parameter is Doppler velocity, determined from the shift of Hα line center. To maximize our Doppler-velocity sensitivity, we apply to the spectra Fourier filtering, interpolation, and padding with zeros at the Nyquist frequency. We then fit the core of the Hα line profile with a parabola. From the shifts of the minima of the fitted profiles of each pixel, we construct Doppler velocity maps; from the intensity of the minima of each pixel we construct line-center spectroheliograms.

In this work we use both true images and spectroheliograms based on scans. We adopt mid-scan times for the MCCD scans and data derived from them (*e.g.*, Doppler velocities, spectroheliograms), and use actual times of exposure for monitor images (which are obtained between scans). Hence, the times of the left and right frames in the movie are not identical.

To clearly see the transient and dynamic events that occurred before the filament eruption, the reader is referred to the MPEG movie contained on the CD-ROM that accompanies this volume (for purposes of review, it can be found at ftp://solar.physics.montana.edu/pub/canfield/solarphys.15nov91.mpeg). These movies have been created from MCCD data obtained from the beginning of MCCD observations $\sim$ 5 hours before the flare until $\sim$ 30 minutes after it. Two types of data are shown. The left panel shows a MCCD image-monitor Hα movie, two frames of which are shown in Figure 1. The right panel shows a cotemporal Doppler-velocity movie derived from the observed Hα line profiles as described above. Red and blue color indicates the amplitude and sign of Doppler velocity (color of Doppler shift). The right and left panels are aligned to within a few arc seconds; As well, the vertical-field inversion lines from the Stokes Polarimeter data, shown in green, allow the reader to relate features seen in the left and right panels. The careful observer will note an artifact that dances around in the stabilized /Ha/ monitor images - a measure of the effects taken out by the image stabilization hardware.

3.2. Crossing fibril morphology and timing

Two types of dark Hα fibrils are seen in the weak-field corridor just north of the filament. The arrow in the left panel of Figure 1 indicates the most common type of dark Hα fibril, an arch filament. The arrow in the right panel of Figure 1 shows the unusual type of fibril, which extends outside the weak-field corridor. As can be seen in Figure 1, it extends across the bright Hα plage north of the filament. Because these unusual fibrils cross the bright Hα plage, we call them crossing fibrils.

The appearance of a crossing fibril is but one stage of a "crossing event" in /Ha. In the first stage, strong blueshifts (and sometimes weaker redshifts, see below) precede the appearance of the crossing fibril. In the second stage, the crossing fibril is visible in absorption in Hα. In the third stage, redshifts appear. The times of these three stages, for those crossing events that are sufficiently well observed to provide adequate topological and temporal sampling, are listed in Table I. The times listed for the crossing fibrils are those at which they are most visible in MCCD monitor images. On the other hand, the times for the Doppler velocity maxima are derived from the spectral data.

Of the crossing events that were observed during the 5-hour period of observations before the eruption, three occurred in the first 2.5 hours of observations and nine occurred in the second 2.5 hours. It is noteworthy that the rate of occurrence was so much greater during the later period. During the first stage coincident transient brightenings (**?**) were frequently observed in soft X-rays, with the SXT. Thus, the crossing event phenomenon is associated with coronal energy release. Some of the observed transient brightenings are orders of magnitude brighter in SXT images than others. We find no unique relationship between the amplitude of the soft X-ray brightening and any property of the crossing event in Hα.

3.3. Crossing event dynamics

The observed crossing events can be described in terms of the three stages of Doppler shift behavior. In the first stage a strong Doppler shift is seen, of order 10 km s^{-1}, which is dominated by blueshifted regions, but sometimes accompanied by redshifts. In the second stage the region of strong Doppler shift propagates, and the crossing fibril becomes visible in Hα. In the third stage only redshifts are seen. During the second stage the Doppler shift regions propagate along the axes of the associated fibrils, reminiscent of the moving blueshift phenomenon discovered after Hα surges (Canfield *et al.*, 1996). Some crossing events also show contiguous redshifts parallel to the region of blueshifts, and the spatial and temporal relationship between the blueshift and redshift regions imply that the emitting material is rotating about an axis parallel to the crossing fibril, as well as rising (again, like the surges observed by Canfield *et al.*, 1996 and filaments observed by Schmieder *et al.*, 1985).

Figure 3 shows the development of two crossing events. The upper half of the figure shows crossing event #8 in Table I. This event is initially dominated by blueshifts (21:48:03 UT). The crossing fibril associated with this event is most evident in the line-center Hα spectroheliograms at 21:51:23 UT, whereas in the velocity maps, the blueshift is most evident at 21:48:03 UT. This tendency for the event to been

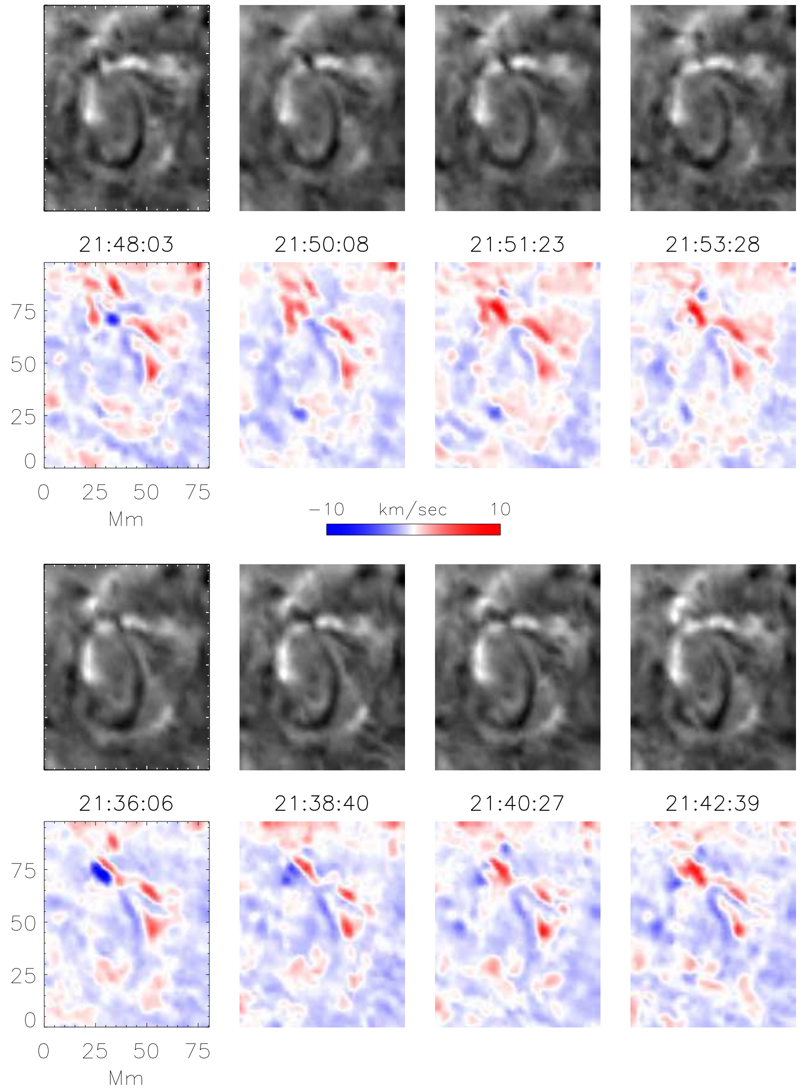

Figure 3. Spectroheliograms and velocity maps during two crossing events. The upper half of the figure shows a crossing event initially dominated by blueshifted pixels (in the 21:48:03 UT color panel, at x,y coordinates $\sim$ 30,70 Mm). The lower half shows one for which both blueshifted and redshifted components are initially seen (in the 21:36:06 UT color panel, at x,y coordinates $\sim$ 30,70 Mm). The first and third rows of the figure are Hα line-center spectroheliograms, the second and fourth rows are Doppler velocity maps.

seen in velocity before it begins absorbing strongly in Hα line center (showing the crossing fibril) is typical. The lower half of Figure 3 shows crossing event #7 in Table I. This crossing event initially exhibits parallel blueshift and redshift regions, although the blueshifts are always somewhat stronger. This indicates that the moving region is approximately cylindrical in form, both rising and spinning around its axis.

Figure 3 also shows that at later times, after the times of maximum visibility of both events, the dynamics of crossing events is dominated by redshifts. At the later times shown in the right-most images in this figure, the redshift region is quite elongated; at even later times, which can be seen in the MPEG movie, the region of redshifts tends to shrink and move northward. Our interpretation of this phenomenon is that the redshift is due to plasma flowing down the legs of the new flux tubes.

The blueshifted regions associated with crossing fibrils are observed to propagate along their axes. This behavior is seen in the MPEG movie at the times of the events listed in Table I. Figure 4 shows the propagation of the blueshift region in event # 7, shown in the top half of Figure 3. Through the grayscale coding of the temporal progression shown in the upper panel, one can see (in the lower left panel) that the region of blueshift starts out north of the magnetic polarity inversion line and ends up in the northwestern part of the filament a few minutes later. The transverse velocity at which the blueshifted region propagates along the fibril toward the filament is $\sim$ 70 km s^{-1}. Propagation toward the filament at such speeds is seen in both types of crossing fibrils, *i.e.*, those that show initial blueshifts alone and those that show both initial blueshifts and redshifts.

Reconnection theory predicts that these whip-like transverse motions along field lines will have velocities of order 0.1 - 1.0 v_A, where v_A is Alfvén speed, $v_A = B/(4\pi\rho)^{-1/2}$, or in conventional units, $v_A = 300(B/100\mathrm{G})/(n_e/10^{12}\mathrm{cm}^{-3})^{-1/2}\mathrm{km\ s}^{-1}$, where B is the magnetic field strength, ρ is the mass density, n_e is the electron number density. For $B = 100$ G and $n_e = 10^{11} - 10^{12}$ cm^{-3}, v_A ranges from 300 to 1000 km sec^{-1}. Hence, the observed 70 km s^{-1} velocity of the torsional motion along the crossing fibril is comparable to what one would expect theoretically for the relaxation to a new equilibrium after reconnection.

3.4. Soft X-ray and Hα morphology

Early in each crossing event (first stage), a transient X-ray brightening (**?**) can be seen in SXT data. Using the white light images from the SXT, MCCD, and HSP, we have co-registered the X-ray and Hα images with the vector magnetograms. An example of such an overlay is shown in Figure 5, for crossing event #4, near the time of maximum soft X-ray brightness. The first blueshift contour is shown at 2.5 km s^{-1}, about three times the noise level in the blueshift signal in the quiet Sun.

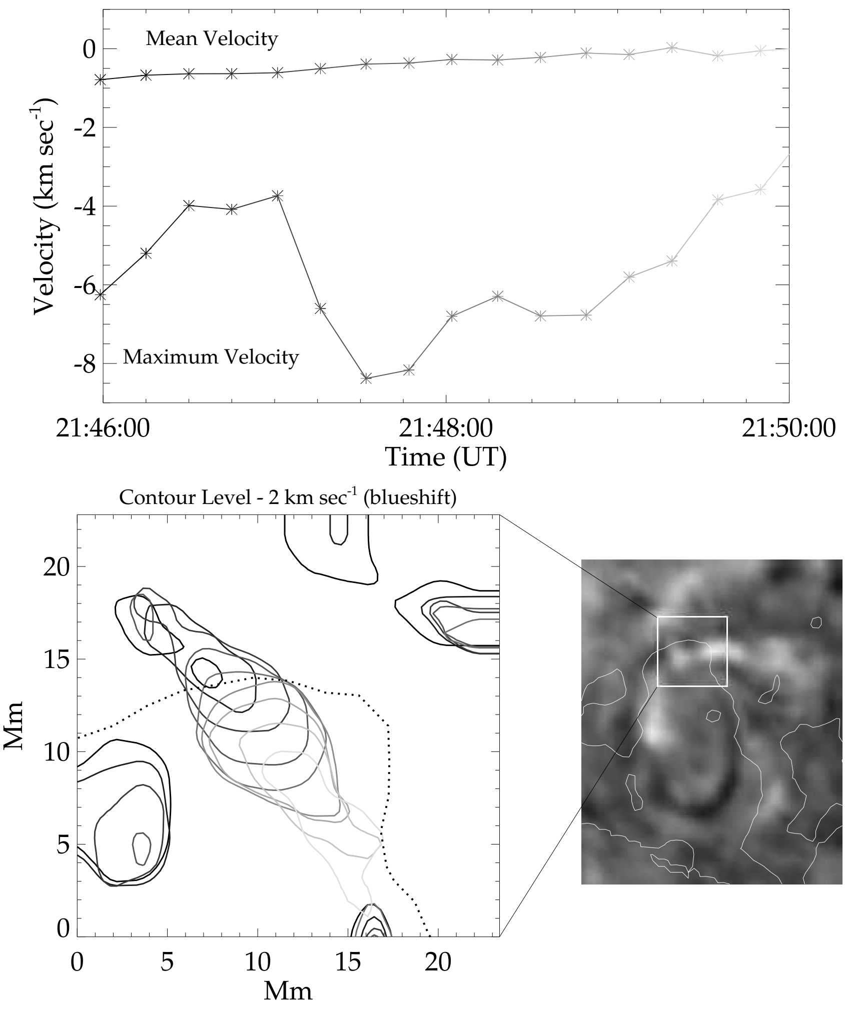

Figure 4. Propagation of the blueshifted feature from the weak-field corridor into the filament along one of the crossing fibrils. The grey-scale temporal coding of the 2 km s^{-1} blueshift velocity contours used in the lower-left panel is given in the upper panel. The dotted line in the lower-left panel is the polarity inversion line of the vertical magnetic field; the part that is shown is at the top of the oval filament, as can be seen from the inset in the Hα line center spectroheliogram shown in the lower right panel. The original data have been rotated so that solar north is up.

The upper region of blueshifts, whose contours are roughly circular in shape, is the first stage of the crossing event, and is close to the region of X-ray emission. After this crossing event, and many other crossing events, the filament undulates. This motion is reflected in the elongated blueshift and redshift contours that overlay the western and southern

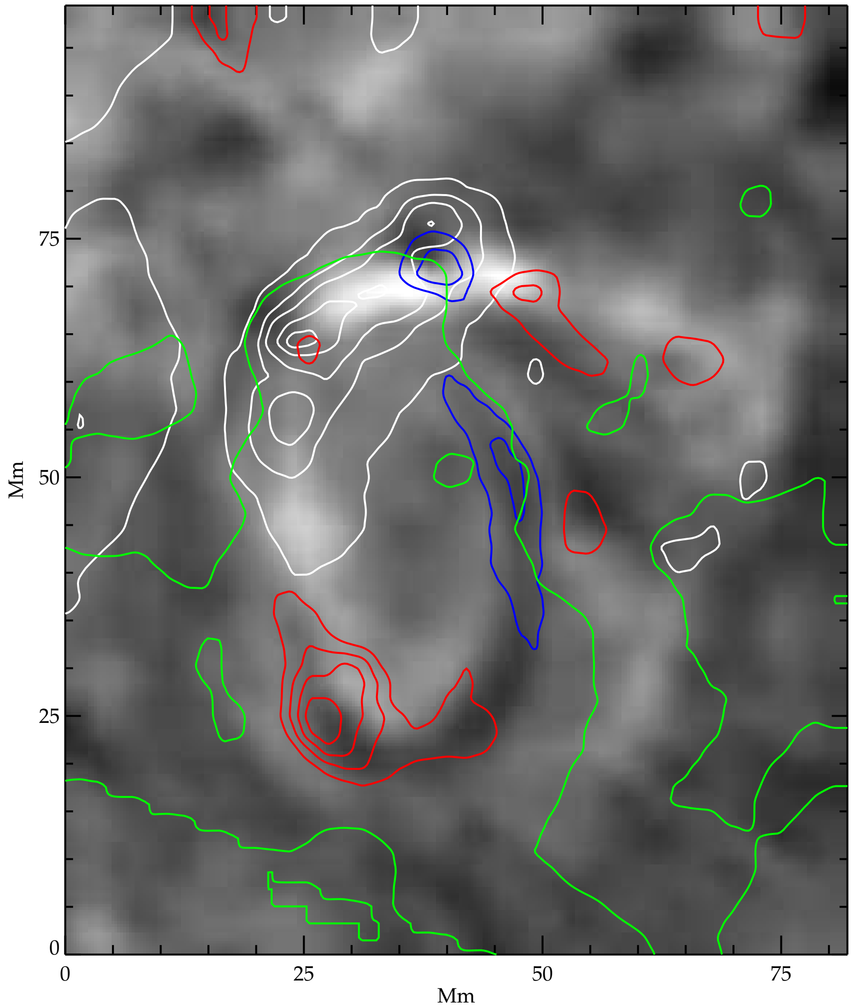

Figure 5. Overlay of the SXT data on the MSO data. Background image – MCCD Hα line-center spectroheliogram, 21:02:44 UT mid-scan time. White contours – SXT Al.1 image at 21:02:38 UT, intensity levels 1000, 3000, 5000, 8000, 10000 DN. Red and blue contours – MCCD Hα redshift and blueshift velocity, $\pm$ 2.5 km s^{-1} interval. Green contours – HSP vertical magnetic polarity inversion lines from an average of the three magnetograms shown above. Solar north is up.

parts of the Hα filament. A small dark Hα feature can barely be seen immediately northeast of the blueshift region that is the first stage of the crossing event. It forms part of a crossing fibril a few minutes later, as can be seen in the movie.

Several Hα and soft X-ray brightenings are seen on both sides of the magnetic polarity inversion line, as is some of the filament. These brightenings are not precisely on the inversion line, but the concept of an inversion line itself breaks down under high resolution. The essential property of the morphology of the event is that the region of initial blueshift is near transient bright /Ha/ and X-ray emissions that span the neutral line.

4. Interpretation

Our interpretation of the crossing events discussed above is that they are the consequence of relaxation and cooling after successive episodes of reconnection of twisted newly-emerged flux with the filament flux system lead to a loss of equilibrium. Figure 6 schematically shows the topology that we infer from the observations. A newly-emerged, twisted flux tube is represented by the arch-filament fibril shown in on the left of the the upper panel (before reconnection) of Figure 6. We observe that the northern extremity of the oval filament flux system is immediately adjacent to the region of flux emergence (Figure 1). We suppose that these two flux systems are actually interleaved, *i.e.*, in three dimensions, the new flux emerges under and among the northernmost field lines in the filament flux system. Hence, these two different flux systems have the opportunity to reconnect, as shown in Figure 6. In Figure 6, we infer that reconnection takes place between and above points B and C, creating a long field line joining footpoints A and D, which we identify with the crossing event, and a shorter one between footpoints B and C, which we associate with soft X-ray and Hα brightenings. Our interpretation of the strong initial velocities in the crossing events is that the long loop has a cusp at the reconnection site at the instant of reconnection, but in a few minutes relaxes to the smooth shape suggested in the lower half of the figure. In the course of this relaxation the cusp region springs up, as evidenced by the transient blue shift seen in Figures 3 and 5. We suppose that some of the arch filaments are twisted at the time of their emergence, as indicated by spiral lines in arch filament shown on the left of the upper half (before reconnection) of the cartoon. In the reconnection process most of this twist is preserved, but in the relaxation process it spreads over both the crossing fibril and the soft X-ray loop. In our interpretation, the propagation of this twist into less twisted filament fibrils is evidenced by presence of spin in some crossing events and its propagation from the weak field corridor into the filament.

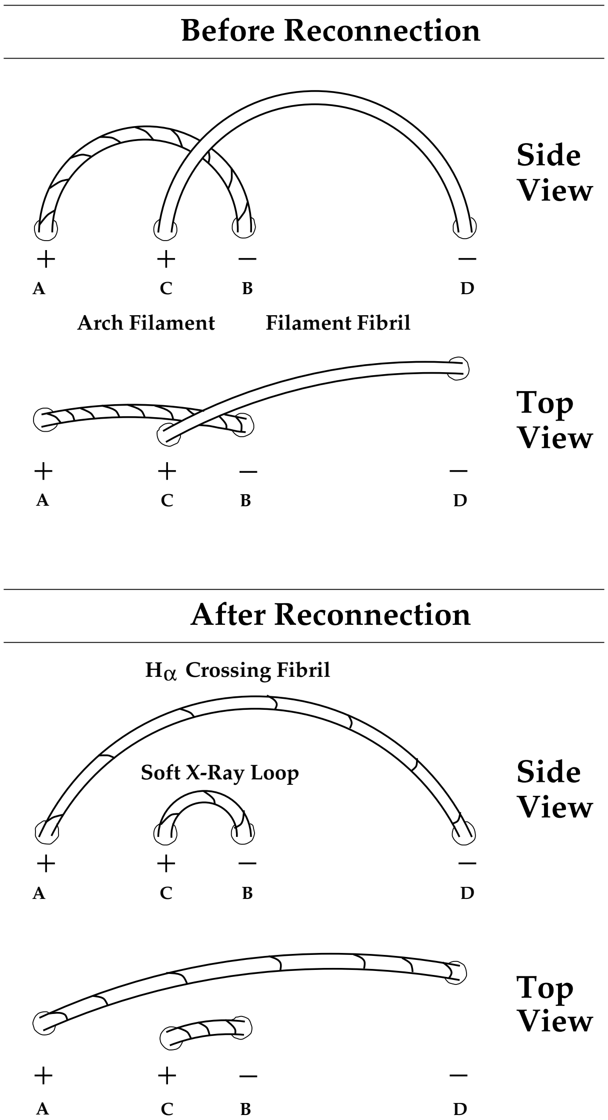

Figure 6. Cartoon model of the relationship between Hα structures (arch filaments, filament fibrils, and crossing fibrils) and the soft X-ray loops of the transient brightenings, before and after reconnection.

When we consider those crossing events that spin, we find that they all do so in the same direction. This then represents the net transfer of this sense of twist from the emerging flux system into the filament flux system during the period of observation. We therefore studied evidence for spinning motions in the eruption itself. We found that there is no obvious evidence that the filament sheds any single sense of twist during the eruption. Instead, the motions of the erupting filament are quite complex; the direction in which the filament spins changes at least three times as one goes around the oval, at the time of onset of strong eruptive motions. Hence, the observations do not support the simple idea that the erupting filament is shedding the twist injected into it by the crossing events.

What do we learn by comparing this to the tether cutting model of Moore and Roumeliotis (1992) and Sturrock? Reconnection, tension, and buoyancy all play a role in that model. In our observations there is evidence (in the morphology, frequency, and dynamics of the crossing fibrils) that successive reconnection episodes of the filament flux system with emerging flux (indicated by the arch filaments and the increasing flux observed in the magnetograms) precede the eruption, as described in the model. As well, there is evidence (in the morphology of the crossing fibrils) that longer field lines are created that are part of the filament flux system, a key aspect of the model. Hence, the events envisioned in the model took place before this flare, and our observations support the phenomenonological aspects of the model. On the other hand, the observations themselves contain no evidence that this enables eruption through reduced tension. Rather, they open the possibility that an important process is addition of twist to the flux system, which is topologically different from merely lengthening its field lines.

Another model with which we should make a comparison is the circuit model of Martens and Kuin (1989). On the basis of this model, the authors argue that there is no unique trigger for filament and flare eruptions, but rather that the filament flux system enters a metastable state prior to the global loss of equilibrium that corresponds to the eruption. In this state any disturbance that is strong enough to move a filament away from its equilibrium state can trigger an eruption. The filament on November 15th shows a tendency to undulate, but not erupt, after each of the crossing events observed during the five hours prior to the eruption. One weak event of twist propagation is seen at the time of the eruption, but it is not compellingly different from any of the similar events that preceded it. It is thus clear that although the crossing events are local, they perturb the system globally.

Both the tether cutting model (Moore and Roumeliotis, 1992) and the circuit model (Martens and Kuin, 1989) contain the idea that the cumulative effects of reconnection with emerging flux can explain the global loss of equilibrium that appears to play a role in this flare. Our observations support this idea. In future work we will make a systematic search of several tens of eruptive flares for which we have MCCD observations to determine whether twist transfer by reconnection is a common, and perhaps useful, precursor of flare eruptions.

Acknowledgements

We thank H. Kurokawa for calling our attention to the evidence for flux emergence prior to this event, D. Rust and A. Pevtsov for stimulating our interest in twist transfer, and D. Longcope for discussions of the mhd kink instability. We thank our Mees and Yohkoh colleagues for their help in securing the observations used in this paper. This research has been supported by NASA through SR&T grant NAG5-5043 and the Yohkoh Soft X-Ray Telescope contract NAS8-40801.

References

Acton, L. W., *et al.*: 1992, Science, 258, 618.
Canfield, R. C. *et al.*: 1992, PASJ, 44, L111.
Canfield, R. C. *et al.*: 1993, ApJ, 411, 362.
Canfield, R. C. *et al.*: 1996, ApJ, 464, 1016.
Dahlburg, R. B., Antiochos, S. K., and Zang, T. A.: 1991, ApJ, 383, 420.
Hudson, H. S., Acton, L. W., Hirayama, T., and Uchida, Y.: 1992, PASJ, 44, 77.
Klimchuk. J. A.: 1987, ApJ, 323, 368.
Kurokawa, H., Hanaoka, Y., Shibata, K, and Uchida, Y.: 1987, Sol. Phys., 108, 251.
Leka, K. D., Canfield, R., C., McClymont, A. N., and van Driel-Gesztelyi, L.: 1996, ApJ, 462, 547.
Martens, P. C. H., and Kuin, N. P. M.: 1989, Sol. Phys., 122, 263.
Mickey, D. L.: 1985, Sol. Phys., 97, 223.
Moore, R. L. and Roumeliotis, G.: 1992, in Z. Svestka, B.V. Jackson, and M.E. Machado (eds.), *Eruptive Solar Flares*, Lecture Notes in Physics, 399, 69.
Ogawara, Y., Takano, T., Kato, T., Kosugi, T., Tsuneta, S., Watanabe T., Kondo, I., and Uchida, Y.: 1991, Sol. Phys., 136, 1.
Penn, M. J., Mickey, D. L., Canfield, R. C., and LaBonte, B. J., 1991, Sol. Phys., 135, 163.
Pevtsov, A. A., Canfield, R. C., and Zirin, H.: 1996, ApJ, 473, 533.
Priest, E. R.: 1984, Solar Magnetohydrodynamics (Dordrecht: Reidel), p. 125.
Sakao, T. *et al.*: 1992, PASJ, 44, L83.
Sakao, T.: 1994, dissertation, University of Tokyo.
Schmieder, B., Raadu, M. A,, and Malherbe, J. M.: 1985, A & A, 142, 249.
Shimizu, T.: 1995, PASJ, 47, 215.
Solar Geophysical Data: 1991, 258, Part I, 34.
Takakura, T. *et al.*: 1995, PASJ, 47, 355.
Tsuneta, S., *et al.*: 1991, Sol. Phys., 136, 37.
van Ballegooijen, A. A. and Martens, P. C. H.: 1989, ApJ, 343, 971.
Vrsnak, B., Ruzdjak, V., Rompolt, B.: 1991, Sol. Phys., 136, 151.
Wülser, J.-P., *et al.*: 1994, ApJ, 424, 459.
Zirin, H.: 1988, *Astrophysics of the Sun*, Cambridge University Press, Cambridge, England, pp. 310 – 313.

Table I. Universal Times of Selected Crossing Events

Event	Blueshift Maximum	Crossing Fibril	Redshift Maximum
1	19:03:29	19:07:26	19:12:12
2	20:26:50	20:33:50	20:37:06
3	20:44:01	20:46:25	20:47:36
4	21:03:30	21:06:10	21:06:50
5	21:10:10	21:14:10	21:18:32
6	21:25:12	21:31:12	21:32:53
7	21:34:41	21:40:10	21:41:38
8	21:47:32	21:51:59	21:52:24
9	21:59:19	22:03:01	22:04:03